





# Ketamine anaesthesia induces gain enhancement via recurrent excitation in granular input layers of the auditory cortex

Katrina E. Deane<sup>1</sup> , Michael G. K. Brunk<sup>1</sup> , Andrew W. Curran<sup>1,2</sup>, Marina M. Zempeltzi<sup>1</sup> , Jing Ma<sup>1</sup>, Xiao Lin<sup>1</sup>, Francesca Abela<sup>1,3</sup>, Sümeyra Aksit<sup>1</sup>, Matthias Deliano<sup>1</sup>, Frank W. Ohl<sup>1,4,5</sup> and Max F. K. Happel<sup>1,4,5</sup> 

<sup>1</sup>Leibniz Institute for Neurobiology, Magdeburg D-39118, Germany

<sup>2</sup>Graduate School of Life Science, Julius Maximilians University, Würzburg D-97074, Germany

<sup>3</sup>University of Pisa, Pisa I-56126, Italy

<sup>4</sup>Institute of Biology, Otto von Guericke University, Magdeburg D-39120, Germany

<sup>5</sup>Center for Behavioral Brain Sciences (CBBS), Magdeburg 39106, Germany

Edited by: Ole Paulsen & Diego Contreras

## Key points

- Ketamine is a common anaesthetic agent used in research and more recently as medication in treatment of depression. It has known effects on inhibition of interneurons and cortical stimulus-locked responses, but the underlying functional network mechanisms are still elusive.
- Analysing population activity across all layers within the auditory cortex, we found that doses of this anaesthetic induce a stronger activation and stimulus-locked response to pure-tone stimuli.
- This cortical response is driven by gain enhancement of thalamocortical input processing selectively within granular layers due to an increased recurrent excitation.
- Time–frequency analysis indicates a higher broadband magnitude response and prolonged phase coherence in granular layers, possibly pointing to disinhibition of this recurrent excitation.
- These results further the understanding of ketamine’s functional mechanisms, which will improve the ability to interpret physiological studies moving from anaesthetized to awake paradigms and may lead to the development of better ketamine-based depression treatments with lower side effects.

**Abstract** Ketamine is commonly used as an anaesthetic agent and has more recently gained attention as an antidepressant. It has been linked to increased stimulus-locked excitability, inhibition of interneurons and modulation of intrinsic neuronal oscillations. However, the functional network mechanisms are still elusive. A better understanding of these anaesthetic

**Katrina E. Deane** is a PhD candidate in the CortXplorer Lab investigating the micro-circuitry of the auditory cortex, the balance of excitation–inhibition, and population and synaptic dynamics. While her analysis language is currently proprietary, she hopes to start moving towards open software and open science during her early career because she believes that is the optimal future. This published study has deepened her appreciation of how brain states are heavily influenced by context and she will consider this when designing experiments. In her current research, she will continue to prioritize analysis of passively awake experimental conditions between anaesthetized recordings and behavioural experiments.



This article was first published as a preprint. Deane K, Brunk MGK, Curran AW, Zempeltzi MM, Ma J, Lin X, Abela F, Aksit S, Deliano M, Ohl FW, Happel MFK. 2019. Ketamine anaesthesia induces gain enhancement via recurrent excitation in granular input layers of the auditory cortex. bioRxiv. <https://doi.org/10.1101/810978>.

network effects may improve upon previous interpretations of seminal studies conducted under anaesthesia and have widespread relevance for neuroscience with awake and anaesthetized subjects as well as in medicine. Here, we investigated the effects of anaesthetic doses of ketamine ( $15 \text{ mg kg}^{-1} \text{ h}^{-1}$ , i.p.) on the network activity after pure-tone stimulation within the auditory cortex of male Mongolian gerbils (*Meriones unguiculatus*). We used laminar current source density (CSD) analysis and subsequent layer-specific continuous wavelet analysis to investigate spatiotemporal response dynamics on cortical columnar processing in awake and ketamine-anaesthetized animals. We found thalamocortical input processing within granular layers III/IV to be significantly increased under ketamine. This layer-dependent gain enhancement under ketamine was not due to changes in cross-trial phase coherence but was rather attributed to a broadband increase in magnitude reflecting an increase in recurrent excitation. A time–frequency analysis was indicative of a prolonged period of stimulus-induced excitation possibly due to a reduced coupling of excitation and inhibition in granular input circuits – in line with the common hypothesis of cortical disinhibition via suppression of GABAergic interneurons.

(Resubmitted 18 February 2020; accepted after revision 16 April 2020; first published online 24 April 2020)

**Corresponding author** K. E. Deane: Brenneckstr. 6 Magdeburg, Sachsen-Anhalt 39118, Germany. Email: katrina.deane@lin-magdeburg.de

## Introduction

In research into cortical function, the use of general anaesthesia aims to prevent acute pain and reduce signal noise, while still leaving the sensory information pathway to the neocortex as intact as possible. Gold-standard studies in this field have therefore historically been performed under anaesthesia or partial anaesthesia (e.g. Hubel & Wiesel, 1959, 1962, 1965, 1969; Heil, 1997*a,b*; Dewese & Zador, 2003; Petersen *et al.* 2003). While technical advances have increasingly allowed us to explore the physiology of cortical functions in awake and behaving animals, still little is known about their direct comparison with anaesthetized states, particularly with respect to the interaction between external stimuli and intrinsic cortical dynamics (Pachitariu *et al.* 2015). A better understanding would help to more accurately interpret findings from both states and therefore have widespread relevance for neuroscience and medicine.

One commonly used surgical anaesthetic in systems physiology is ketamine, an *N*-methyl-D-aspartate (NMDA) receptor antagonist, which enters the open receptor channel, inhibiting ionic exchange (Anis *et al.* 1983; Macdonald *et al.* 1987). A main effect of ketamine is the persistent increase in cortical glutamate which renders cells more excitable (Miller *et al.* 2016; Zhang *et al.* 2019), which is hypothesized as due to disinhibition of the cortex through suppression of GABAergic interneurons (Behrens *et al.* 2007; Homayoun & Moghaddam, 2007; Schobel *et al.* 2013; Miller *et al.* 2016). Synchronization of population dynamics across large cortical distances has been explored *in vivo* through spectral analysis in various human and animal studies: at anaesthetic doses, increased gamma oscillations in cortico-subcortical networks may result from an altered interplay between cortical pyramidal neurons and parvalbumin-expressing

interneurons (Lazarewicz *et al.* 2010; Slovik *et al.* 2017; Grent-<sup>t</sup>-Jong *et al.* 2018; Qi *et al.* 2018). Others found differential effects on neuronal oscillations with decreased large-scale beta band activity at both subanaesthetic (Ma *et al.* 2018; Pallavicini *et al.* 2019) and anaesthetic doses (Hertle *et al.* 2016), and increased theta and decreased alpha EEG (Bojak *et al.* 2013; Blain-Moraes *et al.* 2014). One caveat of current studies comparing cortical processing between anaesthetic and awake states is that they mainly focus on single or multi-unit level data, or on the macroscopic EEG signal in human research. Studies that characterize the mesoscopic scale, and link the observed effects of ketamine to cortical circuitry processing, are still relatively scarce (see Michelson & Kozai, 2018; Fitzgerald & Watson, 2019).

In this study, we compared tone-evoked current-source density (CSD) distributions in the awake and ketamine-anaesthetized ( $15 \text{ mg kg}^{-1} \text{ h}^{-1}$ , i.p.) primary auditory cortex (A1) of male Mongolian gerbils (*Meriones unguiculatus*). The feedforward spatiotemporal current flow of tone-evoked activity across cortical layers is highly similar in the awake and ketamine-anaesthetized A1, suggesting that canonical cortical population activity is conserved during anaesthetic states (Luczak & Maclean, 2012). However, we observed distinct differences in the temporal variability of the overall current flow. Particularly in granular layers III/IV, ketamine led to a significant frequency-specific gain increase by a multiplicative, rather than additive, intracortical amplification (cf. Ferguson & Cardin, 2020). While signal strength increased, peak latencies were shorter, and less variable compared to the awake cortex – indicating higher synchrony of tone-evoked cortical inputs. A continuous wavelet analysis further revealed a larger time–frequency region of phase coherence across trials to incoming

external stimuli. However, the dominant tone-evoked response was mainly attributed to a broadband increase in magnitude reflecting an increase in recurrent excitation previously related to recurrent microcircuits of excitatory neurons in cortical layers III and IV (Liu *et al.* 2007). In this way, ketamine appears to prolong the period of stimulus-induced recurrent excitation due to a reduced coupling of excitation and inhibition in granular input circuits in line with the common hypothesis of cortical disinhibition (Miller *et al.* 2016). Anaesthetic doses of ketamine hamper the high synaptic variability accounting for the probabilistic cortical processing mode in the awake brain, and might therefore be responsible for its effects on consciousness (cf. Supp *et al.* 2011).

## Methods

### Ethical approval

Experiments were conducted in accordance with ethical animal research standards defined by German Law and approved by an ethics committee of the State of Saxony-Anhalt under license 42502-2-1394LIN. They also conform to the principles and regulations of *The Journal of Physiology* as described in by Grundy (2015). All experiments were carried out with adult male Mongolian gerbils (*Meriones unguiculatus*, 4–8 months of age, 70–90 g body weight, total  $n = 20$ ). Female animals were not used as possible variances due to sex was not within the scope of our study.

### Pharmacology

Ketamine–xylazine was administered during surgery and throughout the experiment to maintain a steady level of anaesthesia. Infusion of 45% v/v ketamine (50 mg ml<sup>-1</sup>, Ratiopharm GmbH, Ulm, Germany), 5% v/v xylazine (Rompun 2%, Bayer Vital GmbH, Leverkusen, Germany), and 50% v/v of isotonic sodium chloride solution (154 mmol l<sup>-1</sup>, B. Braun AG, Melsungen, Germany) was given intraperitoneally for an initial dose of 0.004 ml g<sup>-1</sup> body weight. A needle was placed subcutaneously to maintain anaesthetic status with an infusion rate of 22 mg kg<sup>-1</sup> h<sup>-1</sup> for deeper anaesthesia during the surgery and a rate of 15 mg kg<sup>-1</sup> h<sup>-1</sup> during the experiment for acute recordings. Anaesthetic status was regularly checked (every 10–15 min) by paw withdrawal reflex and breathing frequency. Body temperature was kept stable at 34°C. In acute recordings, a final dose was administered subcutaneously at the end of the experiment and animals were sacrificed by decapitation.

### Electrophysiological recordings

We recorded activity from the A1 of either animals that received ketamine–xylazine anaesthesia, by acute

implantation of a recording electrode ( $n = 11$ ), or from awake and passively listening animals, with chronically implanted electrodes ( $n = 9$ ).

### Acute recordings and pharmacological silencing of the auditory cortex

The surgical procedure for electrophysiological recording has been previously described in detail (Deliano *et al.* 2020). Briefly, ketamine–xylazine was administered as described above – before and throughout the surgery and experiment. The right auditory cortex was exposed by trepanation and the A1 was located by vascular landmarks. A small hole was drilled on the contralateral hemisphere for implanting a stainless-steel reference wire (Ø 200 µm). Animals were head-fixed with an aluminum bar, affixed by UV-curing glue (Plurabond ONE-SE and Plurafill flow, Pluradent, Offenbach, Germany).

Animals were head-fixed in a Faraday-shielded acoustic soundproof chamber with a speaker located 1 m posteriorly (Tannoy arena satellite KI-8710-32, Tannoy, London, UK). Local field potentials (LFPs) were recorded with a 32-channel shaft electrode (A1x32-50-413, NeuroNexus, Ann Arbor, MI, USA) implanted in the A1 perpendicular to the cortical surface (Happel *et al.* 2010). Recorded LFPs were fed via an Omnetics connector (HST/32V-G2O LN 5V, 20× gain, Plexon Inc., Dallas, TX, USA) into a PBX2 preamplifier (Plexon Inc.) to be pre-amplified 500-fold and band-pass filtered (0.7–300 Hz). Data were then digitized at a sampling frequency of 1000 Hz with the Multichannel Acquisition Processor (Plexon Inc.).

A series of pseudo-randomized pure-tone frequencies covering a range of seven octaves (tone duration: 200 ms, inter-stimulus interval: 800 ms, 50 pseudo-randomized repetitions, 65 dB sound pressure level, 7.5 min per measurement, 125 Hz to 32 kHz). We determined the best frequency (BF) as the frequency evoking the strongest response in the averaged granular CSD channels (see below). Stimuli were generated in Matlab (R2006b, The Mathworks, Natick, MA, USA), converted into analog (sampling frequency 1000 Hz, NI PCI-BNC2110, National Instruments, Austin, TX, USA), routed through an attenuator (g-PAH, Guger Technologies, Graz, Austria), and amplified (Thomas Tech Amp75, Tom-technology, Ilirska Bistrica, Ljubljana). A microphone and conditioning amplifier were used to calibrate acoustic stimuli (G.R.A.S. 26AM and B&K Nexus 2690-A, Brüel & Kjær, Naerum, Denmark).

Recordings of tone-evoked responses were taken after recording quality had stabilized, typically 2 h after implantation. After measuring the tonotopic tuning, 20 µl of the GABA<sub>A</sub> agonist muscimol (8.23 mM muscimol, Tocris Bioscience, Bristol, UK, batch no: 9C/107090), dissolved in isotonic sodium chloride solution, was applied

topically onto the cortical surface, a method introduced and quantified by Edeline *et al.* (2002), to silence intracortical contributions of synaptic activity (Happel *et al.* 2010). Once the muscimol had diffused through all cortical layers, residual thalamocortical inputs could still be detected by early current sink inputs in layers III/IV and Vb/VIa. Tonotopic tuning of isolated thalamocortical inputs was performed as before cortical silencing.

### Chronic implantation and *in vivo* tonotopy recording

Chronic implantation of a recording electrode followed similar surgical procedures to those for acute implantation. Importantly, the trepanation was kept smaller in order to limit the region of exposed cortex to avoid tissue damage and to achieve stable fixation of the electrode later. A recording electrode with a flexible bundle between shaft and connector (NeuroNexus, A1x32–6mm-50-177\_H32\_21mm) was inserted and an initial recording was conducted in order to guarantee the implantation within A1. Then, the electrode and the connectors (H32 Omnetics, Minneapolis, MN, USA) were both glued to the skull with a UV-curing glue (Plurabond ONE-SE and Plurafill flow, Pluradent, Offenbach, Germany). In order to protect the small exposed region of the cortex, the hole was filled with a small drop of an antiseptic lubricant (K-Y Jelly, Reckitt Benckiser, Slough, UK). After the surgical procedure, animals received analgesic treatment with Metacam (i.p. 2 mg kg<sup>-1</sup> body weight; Boehringer Ingelheim GmbH, Ingelheim am Rhein, Germany) administered together with 5% glucose solution (0.2 ml). Animals were allowed to recover for at least 3 days before the first recording.

Animals were then placed in a single-compartment box in an electrically shielded and sound-proof chamber. Recordings were performed with the head-connector of the animal through a preamplifier (HST/32V-G2O LN 5V, 20× gain, Plexon Inc. or RHD2132 Omnetics, Intan Technologies, Los Angeles, CA, USA) and a data acquisition system (Neural Data Acquisition System Recorder Recorder/64, Plexon Inc. or RHD2000 series, Intan Technologies), visualized online (NeuroExplorer, Plexon Inc. and RHD2000 interface GUI software, Intan Technologies), and stored. Broadband signals were filtered offline to extract local field potentials (2000 Hz sampling frequency and later downsampled to 1000 Hz). Acoustic stimuli were presented with the same parameters as in the anaesthetized group. Auditory stimuli were calibrated using a 1/2-inch condenser microphone (Brüel & Kjær) and presented with an intensity of 20 dB above a detectable averaged tone-evoked LFP component. Stimuli were digitally synthesized and controlled using Matlab (R2012b) and presented by Presentation® (Neurobehavioral Systems, Berkeley, CA, USA). Stimuli were delivered via an attenuator (g-PAH, Guger Technologies),

an amplifier (Lehmann Audio, Köln, Germany) and two electrostatic loudspeakers positioned 5 cm outside both sides of the box.

### Current source density analysis

Based on the recorded laminar local field potentials, the second spatial derivative was calculated in Matlab (R2016a), yielding the CSD distribution as seen in eqn (1):

$$\text{CSD} \approx \frac{\delta^2 \Phi(z)}{\delta z^2} = \frac{\Phi(z + n\Delta z) - 2\Phi(z) + \Phi(z - n\Delta z)}{(n\Delta z)^2} \quad (1)$$

where  $\Phi$  is the field potential,  $z$  is the spatial coordinate perpendicular to the cortical laminae,  $\Delta z$  is the sampling interval, and  $n$  is the differential grid (Mitzdorf, 1985). LFP profiles were smoothed with a weighted average (Hamming window) of seven channels which corresponds to a spatial kernel filter of 300  $\mu\text{m}$  (Happel *et al.* 2010). CSD distributions reflect the local spatiotemporal current flow of positive ions from extracellular to intracellular space evoked by synaptic populations in laminar neuronal structures. Current sinks thereby correspond to the activity of excitatory synaptic populations, while current sources mainly reflect balancing return currents. Early synaptic thalamocortical inputs persist after intracortical silencing with the GABA<sub>A</sub> agonist muscimol related to thalamocortical projections on cortical layers III/IV and Vb/VIa (Happel *et al.* 2010; Happel & Ohl, 2017; Brunk *et al.* 2019) in accordance with reports by others (Schaefer *et al.* 2015). Early current sinks in the auditory cortex are therefore indicative of thalamic input in granular layers III/IV and infragranular layers Vb/VIa (Szymanski *et al.* 2009; Happel *et al.* 2010).

CSD profiles were further transformed by averaging the rectified waveforms of each channel:

$$\text{AVREC} = \frac{\sum_{i=1}^n |\text{CSD}_i| (t)}{n} \quad (2)$$

where  $n$  is the individual channel and  $t$  is time in milliseconds. This average rectified (AVREC) measure gives us the overall temporal local current flow of the columnar activity (Givre *et al.* 1994; Schroeder *et al.* 1998).

Based on tone-evoked CSD distributions, we assigned the main sink components to the cortical anatomy as follows: the early dominant sink components are attributed to lemniscal thalamocortical input, which terminates in cortical layers III/IV and Vb/VIa (Fig. 1; see Happel *et al.* 2010). Subsequent sink components emerge in supragranular layers I/II, and infragranular layers Vb and VIa.

### Clustermass permutation analysis

To compare CSD profiles for BF stimulation and 2 octaves away (BF-2), clustermass permutations were performed between the CSD data of ketamine-anaesthetized and awake recordings – a test specifically suited to control specifically for a familywise error rate (Groppe *et al.* 2011). The groups were averaged and then a difference (ketamine minus awake) was calculated for the observed CSD matrices. We extracted a *t*-statistic pointwise across CSD profiles of groups: ketamine and awake (total of  $32 \times 600$  Student's *t* tests). We selected a *t*-threshold based on a two-tailed *P*-value of 0.05 or less using the group sizes to calculate degrees of freedom. Any *t*-statistic at or above this 'significance' threshold was converted to a 1 and anything below was converted to a 0 – creating a binary matrix of 0s and 1s, in which 1 is a possible point of significance in the comparison of awake CSD profiles against ketamine-anaesthetized CSD profiles. The 1s were then summed to create our observed clustermass value. Next, we permuted the groups 'awake' and 'ketamine-anaesthetized' 1000 times; condition containers were equal to observed group sizes (11 and 9 subjects) and the CSD profiles from the ketamine and awake groups were randomly allocated into those containers. The same point-wise *t*-statistic and threshold calculated binary map was produced for each permutation with the total sum of 1s for each taken as

a permutation clustermass. This created a distribution of 1000 permutation clustermass values over randomized conditions, awake and ketamine-anaesthetized, to which the observed clustermass could be compared. A *P*-value was calculated according to where the observed clustermass value fell onto the permutation distribution. This entire process was performed on the full CSD profile vertically spanning the cortical column as well as on layers I/II, III/IV, Vb and VIa. These were selected based on the averaged CSD profile's overlapping centre layer channels to avoid analysing between different cortical layers.

### CSD-derived tuning curves

Tuning curves of layer-wise tone-evoked activity were centred on the BF response of each respective layer. Tuning curves were calculated for root mean square (RMS) values and peak latencies. Values were detected automatically when the sink activity crossed 1.5 standard deviations below the measured baseline activity. Candidate sink components were detected within each layer for an early time window (1–65 ms after tone onset) and a late time window (66–400 ms after tone onset). Based on the RMS power, the strongest sink activation was selected per time window.

Tuning curves for average rectified CSD (AVREC) were centred on the BF of the granular thalamocortical sink

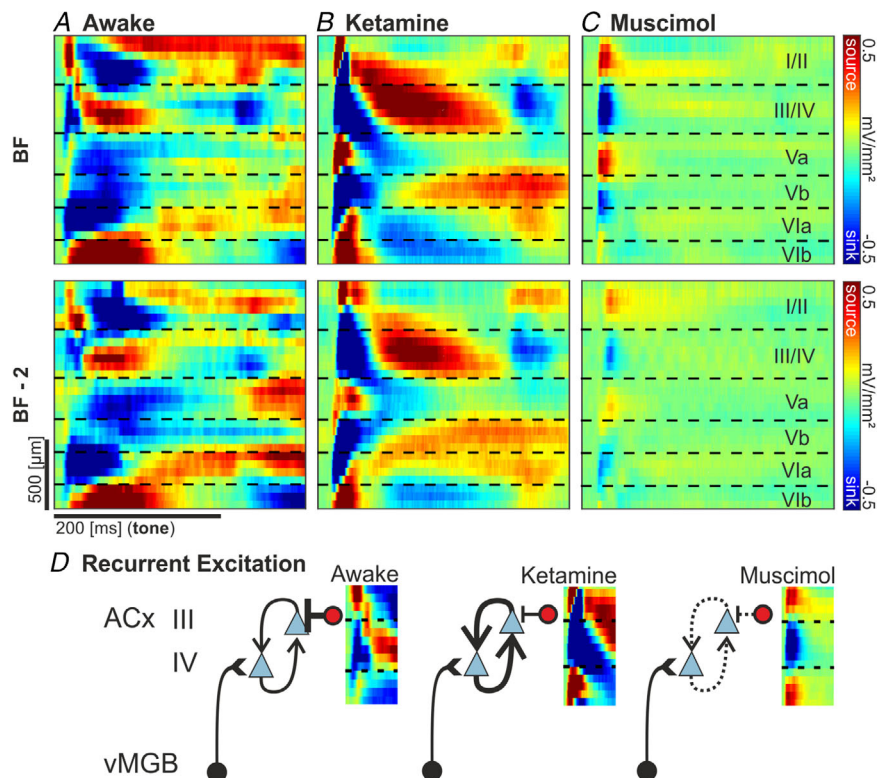


**Figure 1. Grand average current-source density profiles**  
 A–C, BF and BF -2 in awake (A), ketamine (B), and muscimol conditions (C) (*n* = 9, 11 and 11, respectively). Top, best frequency response. Bottom, response 2 octaves below the best frequency. The CSD shows the pattern of temporal processing (ms) at cortical depths (μm). Representative layer assignment is indicated with horizontal dashed lines corresponding to the layers in C. Pure-tone stimuli are presented for the first 200 ms. Current sinks (blue) represent areas of excitatory synaptic population activity, while current sources reflect balancing currents (Happel *et al.* 2010). D, diagram of the potential contribution of cortical recurrent excitation in layers III/IV and its presumed balance differences in each of the 3 tested conditions.

(layer III/IV). Tuning features at the columnar level were calculated within the first 100 ms of tone presentation as RMS amplitude, peak amplitude and peak latency.

### Continuous wavelet transform

Spectral analysis was performed in Matlab (R2019a) using the wavelet analysis toolbox function CWT for the following variables: animal, condition, stimulus and recording channel. Important parameters fed into the CWT are as follows: CSD profiles, frequency limits: 5–100 Hz (below the Nyquist); and wavelet used: analytic Morse (see Olhede & Walden, 2002; Lilly & Olhede, 2012). For layer-wise wavelet analysis, three channels centered on the middle channel of each layer were fed into the CWT and averaged. A trial-averaged scalogram was calculated for each cortical layer and wavelet magnitude – per frequency, per time point – for each subject was computed with eqn (3).

$$\text{Magnitude} = |a + b_i| \quad (3)$$

where  $a + b_i$  represents the complex number output of the trial-averaged CWT analysis. Single trial scalograms were calculated for each animal as well and phase coherence – per frequency, per time point – for each subject was computed with eqn (4).

$$\text{Phase coherence} = \left| \frac{\sum (a+b_i) / |a+b_i|}{n} \right| \quad (4)$$

where  $a + b_i$  represents the complex number output of the single trial CWT analysis (Lachaux *et al.* 1999). Magnitude and phase coherence data were averaged pointwise (i.e. frequency and time bins are consistent across averages) for group plots. Clustermass permutations (as above) were performed for the difference between spectral representation in each layer at the BF and two octaves below (BF –2). Frequency bands were split as follows: theta 4–7 Hz, alpha 8–12 Hz, low beta 13–18 Hz, high beta 19–30 Hz, low gamma 31–60 Hz, and high gamma 61–100 Hz. For magnitude calculations, the statistical test for permutation was Student's *t* test, and Cohen's *d* matrix was generated to indicate effect size per frequency at each time point. For phase coherence calculations, the statistical test for permutation was the non-parametric Mann-Whitney *U*-test (toolbox from Matlab file exchange: Maris *et al.* 2007; Cardillo, 2009) and effect size was indicated with the *z*-score output as follows:

$$U \text{ test Effect Size} = \left| \frac{Z}{\sqrt{n}} \right| \quad (5)$$

## Results

### Altered spatiotemporal profile in the auditory cortex induced by ketamine anaesthesia

We compared the tone-evoked laminar CSD profiles in the primary auditory cortex of Mongolian gerbils under ketamine–xylazine anaesthesia, with cortical silencing by topical application of muscimol, and while awake (Fig. 1). Comparison of pure-tone-evoked grand averaged CSD profiles revealed distinct differences in the spatiotemporal flow of synaptic activity across cortical layers. CSD profiles of both groups (Fig. 1A and B) were characteristic of the spatiotemporal flow of sensory information across cortical layers in line with previous findings (Barth & Di, 1990; Steinschneider *et al.* 1992, 1998; Sakata & Harris, 2009; Szymanski *et al.* 2009; Atencio & Schreiner, 2010). Approximately 15–20 ms after pure-tone onset, an initial sink component was detected in granular layers III/IV as well as infragranular layers Vb and VIa, all originating from lemniscal feedforward thalamocortical projections to A1 (Happel *et al.* 2010). From these input circuits, synaptic population activity propagates to supragranular and infragranular layers yielding later sink components (Chen *et al.* 2007; Sakata & Harris, 2009; Atencio & Schreiner, 2010; Schroeder *et al.* 1998). This columnar activation was more robust under BF stimulation and less when stimulating with a frequency two octaves below (BF–2; cf. Metherate *et al.* 2005; Happel *et al.* 2010). Overall, Fig. 1 reveals a similar spatiotemporal pattern of auditory-evoked responses with respect to the order of current sinks across layers and time in awake animals and under ketamine anaesthesia. A qualitative comparison reveals a weaker and less expanded early granular sink component and more temporal spread of subsequent current sink components in the awake state. This might be indicative of a ketamine effect on thalamic input activity and recurrent excitation possibly due to disinhibition causing less variable and more stimulus time-locked activity. Figure 1D shows a diagram of hypothesized recurrent excitation effects corresponding to CSD profiles.

In order to disentangle thalamic input to the cortex from further cortico-cortical processing, the GABA<sub>A</sub> agonist muscimol was applied topically to the auditory cortex (Happel *et al.* 2010). Muscimol silenced all intracortically generated activity in the cortex except for the short thalamic inputs in granular and infragranular layers (Fig. 1C). The strength of the early granular sink activity was strongly reduced and shorter under muscimol, reflecting the strong intracortical amplification of early thalamic input under ketamine. Consistently, the spatial width of the granular thalamic sink was reduced under muscimol, indicating that the immediate recurrent excitation in cortical layers III/IV was being blocked by the drug. A comparable reduction of strength

and width of tone-evoked activity after silencing intracortical processing could be observed in the early infragranular sink component. Disentangled thalamic input components to the cortical activity pattern were slightly less strong for frequencies two octaves below the BF. Qualitative differences between the awake and ketamine group (Fig. 2A) were tested for significance via a cluster-mass permutation test (Fig. 2B). A comparison of the entire CSD matrix showed that there was a significantly higher cluster-mass in the observed measurements than in the distribution of permutations. An analysis of cortical layer activity separately revealed that activation in layer III/IV is highly significantly different across conditions. Less pronounced were significant differences in layers I/II, Vb and VIa. The purpose of this permutation test was to validate that effects illuminated by further statistical methods are unlikely to be randomly produced, which is particularly the case for cortical layers III/IV.

### Ketamine strengthens stimulus-locked activity by reduced temporal variability of tone-evoked input

The CSD profiles of the awake and ketamine groups indicated temporal differences of tone-evoked activity

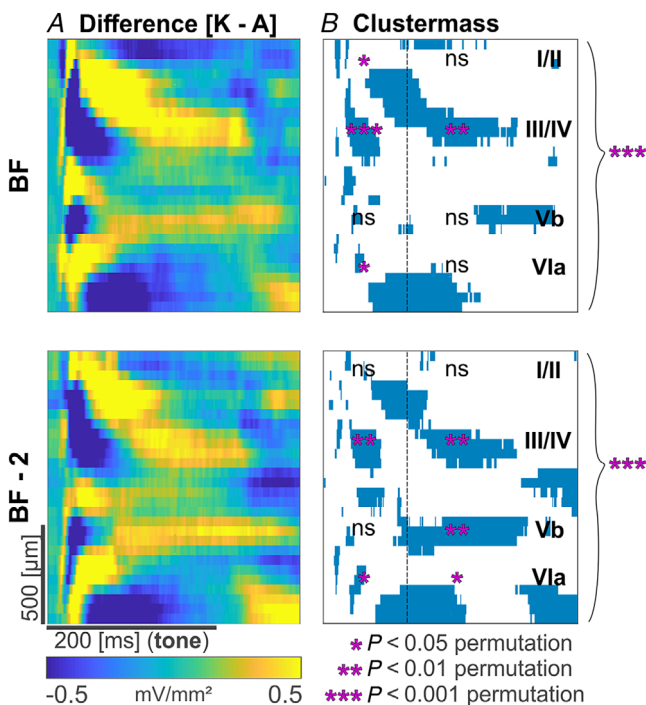


**Figure 2. CSD cluster-mass permutation test**

A, the difference (ketamine – awake) between the grand averaged CSD profiles for BF and BF – 2 octaves. B, observed cluster-mass of significant differences ( $P < 0.05$ ) are plotted in blue (verified by a two-sample Student's  $t$  test). Significances ( $*P < 0.05$ ,  $**P < 0.01$ ,  $***P < 0.001$ ) of the permutation test are indicated by asterisks. Comparisons of the permutation test have been performed for early (1–100 ms) and late (101–400 ms) signals on a layer-wise (I/II, III/IV, Vb, VIa) and columnar level (indicated by braces on the right side).

(Fig. 1). We therefore compared the group's AVREC traces (Fig. 3A) as a measure of the temporal current flow between groups. Ketamine-anaesthetized subjects showed stronger AVREC onset response peaks. This is indicative of a more stimulus-onset-locked activation of the cortical microcircuitry. Muscimol reduced the response strength but demonstrated a similar pattern of time-locking with BF stimulation. Stimulation with frequencies 2 octaves apart from the BF generated only a slightly detectable tone-evoked component. Awake subjects show a broadened response after stimulation with both the BF and the BF – 2. In order to quantify these effects, we further calculated tuning parameters at a single-trial level (Fig. 3B). Consistently, under ketamine single-trial peak amplitudes were significantly higher compared to the awake group for all stimulation frequencies (Fig. 3B, left). The amplitude increase might be due to a higher precision of the stimulus-locked activity which is further implied by a lower variability of the peak latencies in the ketamine group (Fig. 3B, middle).

In order to confirm consistency of these findings across animals, we also compared data measured under ketamine anaesthesia while implanting the chronic electrodes in the subjects of the awake group (data not shown). While the columnar CSD-derived tone-evoked activity was highly comparable between the ketamine-anaesthetized group and recordings during implantation, we found a period of stabilization of cortical activity under anaesthesia that took roughly 1 h. We opted to compare data between awake and anaesthetized recordings considering this time window.

After muscimol silencing, peak latencies were even faster with less overall strength of the evoked peak amplitude. Muscimol also led to a reduced tuning width around the BF due to a lack of prominent peaks during the detection window of 1–100 ms after tone onset. This can be explained by the silenced intracortical circuitry which normally broadcasts spectral information across the cortical space (Kaur *et al.* 2004). The RMS of the AVREC waveform resembled not the highest activation, but the summed activity over time. Within the first 100 ms after tone onset we observed a strong significant difference in the ketamine-anaesthetized group before and after muscimol treatment (Fig. 3B, right). However, the Cohen's  $d$  effect size between the awake and ketamine group showed that the RMS does not differ – indicating that the current flow over time between the awake and ketamine group was rather comparable despite such a strong difference between the peak amplitudes and latencies.

The higher overall AVREC peak amplitude, shorter peak latencies and small Cohen's  $d$  of RMS activity under ketamine anaesthesia might be explained by a more synchronized recruitment of synaptic circuits. We therefore assumed that the variance of evoked amplitudes would be higher under ketamine anaesthesia,

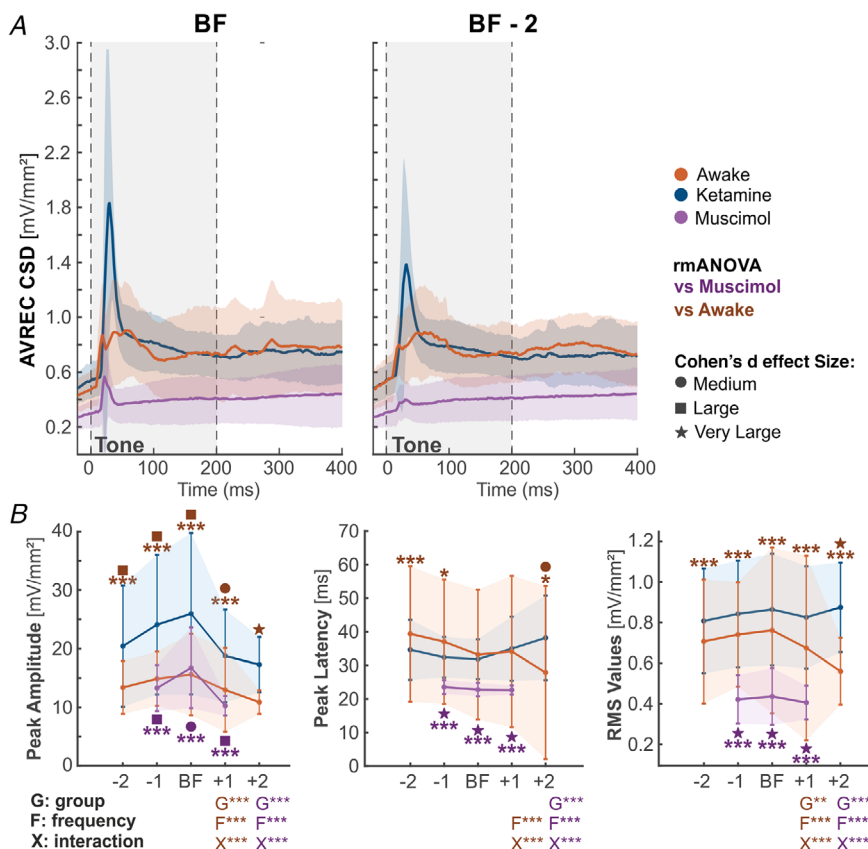
while responses peak latencies were more distributed in awake recordings (Fig. 4A). To test this, we applied a Brown–Forsythe test of variance to characterize noticeable differences in variance between timing and amplitude of the peaks of each group. Under ketamine anaesthesia, there was a significantly larger variance in peak amplitude compared to both awake ( $P < 0.001$ ) and with muscimol ( $P < 0.01$ ; Fig. 4B). Conversely, awake subjects had significantly higher variance at peak latencies ( $P < 0.001$ ; Fig. 4B). This analysis accounted for the temporally broader shape of the grand-averaged AVREC responses in the awake condition compared to ketamine-anaesthetized subjects exhibiting a more stimulus-locked overall activity pattern.

### Ketamine-induced gain increase is due to amplitude effects on granular input layer activity

In order to identify the source of the overall columnar differences, laminar tuning curves were calculated for various parameters of detected current sinks for each animal at thalamocortical input layers III/IV, Vb and VIa, and supragranular layers I/II (Fig. 5). The main effect on the evoked peak amplitude described for the AVREC waveform was reflected by the RMS value in granular input layers. Here, ketamine anaesthesia also led to an increase across all stimulation frequencies. Infragranular layer Vb

and VIa showed no clear difference of the evoked RMS value (Fig. 5A). In contrast, the longer peak latencies of the AVREC waveform were reflected mainly in the temporal activity of supragranular layers. Here, peak latencies had large or very large effect sizes in the awake animals for most stimulation frequencies (Fig. 5B). Peak latencies of other sink components showed only minor differences. This analysis of layer-specific sink activity revealed that the main drive for the time-locked columnar activity and higher peak amplitudes under ketamine was a strong excitation in cortical input layers III/IV. The increase of the layer III/IV RMS value appeared to be mostly a modulation of gain paired with only a minor difference in tuning sharpness between the awake and ketamine group. In order to reveal the frequency specificity of such multiplicative gain, we calculated RMS values of current sink activity measured in individual layers binned for stimulation frequencies with 1 or 2 octave distance from the BF and normalized to the BF response strength (Fig. 5C). Sink activity in cortical layers I/II, III/IV and Vb showed a corresponding frequency-specific gain increase with the effects being significant in the granular layer.

In order to differentiate effects of amplitude and phase-locking on the described gain effects implicated by our data, we used continuous wavelet analysis (Figs 6 and 7) at a laminar level to quantify the spectral representation between groups. In general, the spectral





magnitude in granular layers III/IV showed the highest difference between both groups with an increase in magnitude across all spectral bands in the ketamine group for BF stimulation (Fig. 6A). This broadband significant increase between ketamine-anaesthetized and awake CSD scalograms was not present at BF -2, indicating more similar tuning curves for both groups at border frequencies (Fig. 5). The significant increase in magnitude for BF stimulation was revealed by a high Cohen's *d* effect size and with a permutation clustermass test for all frequencies from theta (4–7 Hz) to high gamma (60–100 Hz). The nature of this broadband magnitude increase in cortical layers III/IV induced by ketamine was consistent with the immediate recruitment of synaptic activity indicating stimulus-locked gain increase. In other layers, magnitude effects were less pronounced. In Fig. 6B, the supragranular I/II and infragranular VIa clustermass permutation tests revealed no areas of significant magnitude increase above chance. Layer Vb shows an increase across low and high beta and low gamma.

Further, we analysed single trial phase coherence for the corresponding individual layer-wise CSD traces

(Fig. 7). While ketamine increased the stimulus-induced magnitude most prominently at stimulus onset, its effects on phase coherence were mainly around the time of stimulus-induced columnar response. A corresponding broadband increase in phase coherence across all frequency bands as well as a strong increase in the lower beta range proceeded during stimulus presentation above chance according to permutation (Fig. 7A). Beta phase coherence was also significantly increased above chance in thalamocortical input layer Vb. Effects were less prominent in cortical layers I/II and VIa (Fig. 7B).

### Discussion

We investigated the effects of anaesthetic doses of ketamine (15 mg kg<sup>-1</sup> h<sup>-1</sup>) on synaptic population dynamics in the auditory cortex of Mongolian gerbils using layer-specific CSD analysis. We intended to illuminate functional mechanisms under ketamine anaesthesia which would benefit translational research on using it as a therapeutic agent. Our data revealed a cortical gain increase under ketamine driven by a stronger recruitment of layer

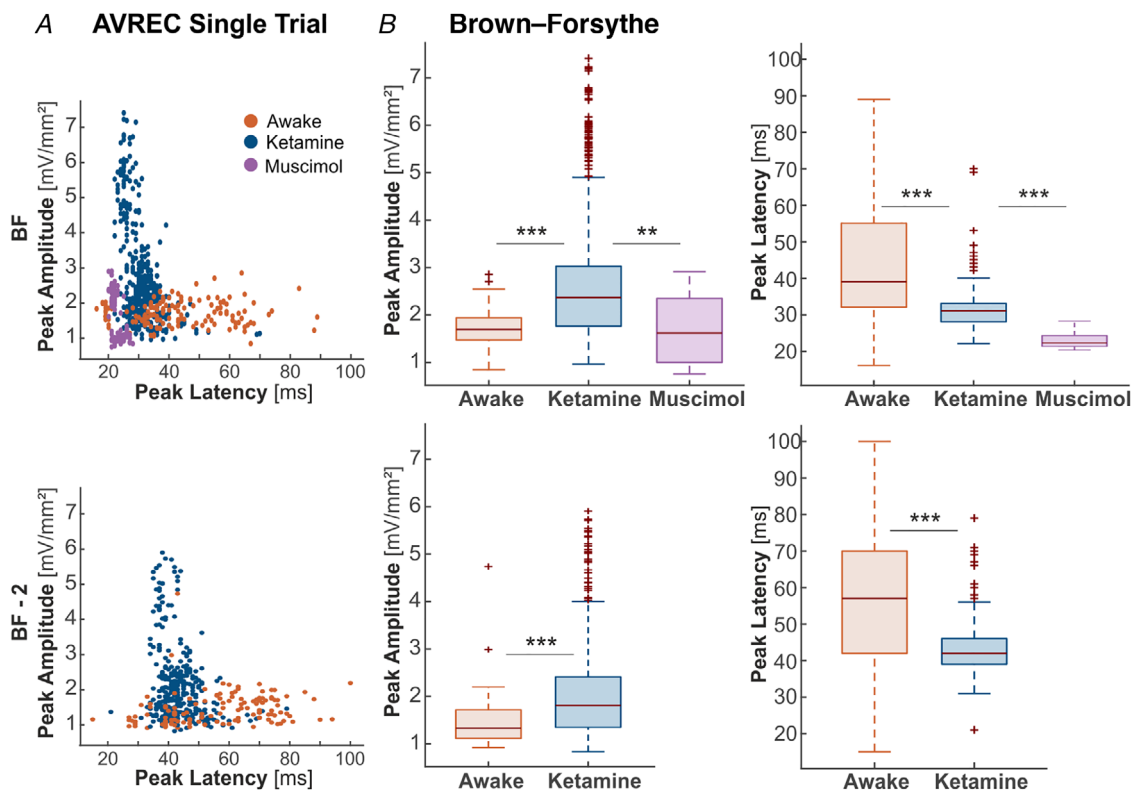


**Figure 4. Brown-Forsythe test of variance for peak amplitude and latency**  
 A, single trial-based scatter plots of amplitude against latency of detected AVREC CSD peaks at BF (top) and BF -2 (bottom). B, Brown-Forsythe variance plotted as boxplots for awake (orange, *n* = 9), ketamine (blue, *n* = 11), and muscimol (purple, *n* = 11) groups for peak amplitudes (left) and latencies (right). Boxes represent the 25% quartiles, the bar represents the median, and whiskers represent the full range of data except for outliers plotted as crosses. Note that cortical silencing via muscimol reduces measurable activity in non-BF stimulations. \*\*\**P* < 0.001, \*\**P* < 0.01

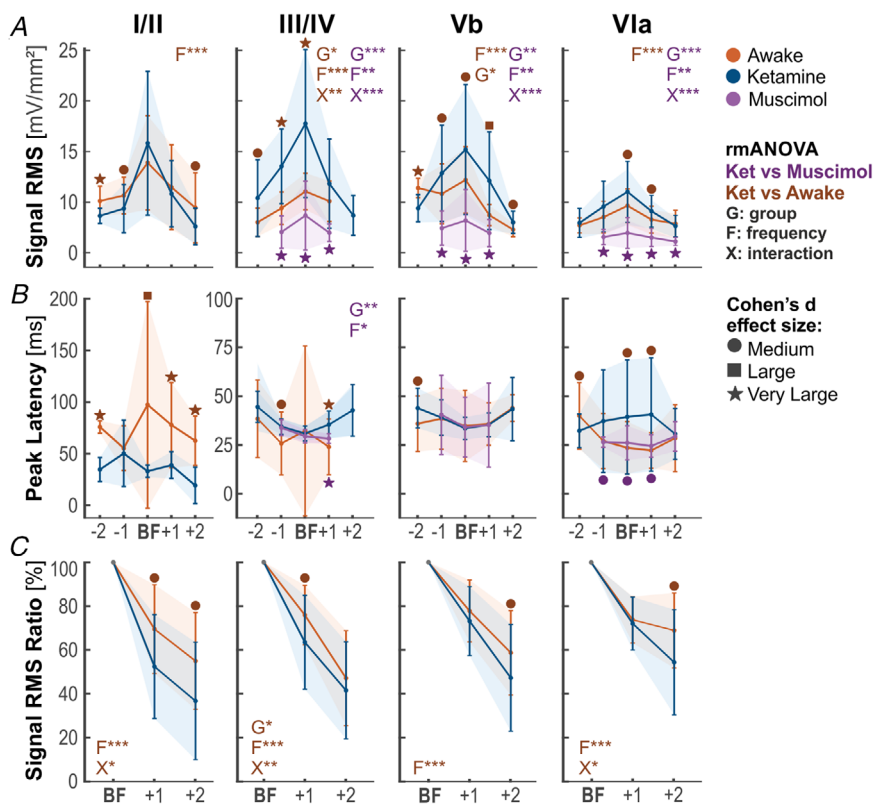
III/IV. This was ascribed to an increase in tone-evoked amplitude across spectral frequencies in a continuous wavelet (CWT) analysis rather than stimulus–response phase locking. Ketamine produced an area of higher phase coherence to incoming stimuli mainly in granular layers in comparison to a more variable signal response in awake animals, but this difference was not significant during early thalamocortical input processing. We observed higher stimulus-locked responses at more variable amplitudes under ketamine, specifically in granular thalamic input layers. Our findings therefore argue for an altered input processing due to an increase in recurrent excitation of thalamocortical inputs selectively in granular layers III/IV which may be attributed to a disinhibition of GABAergic interneurons, leading to a reduced coupling of excitatory and inhibitory input circuits under ketamine.

### Ketamine induces a higher time-locked stimulus response at more variable peak amplitudes

Ketamine reduced the variability of early thalamocortical input in granular layers, which accounts for the stimulus-locked response strength and, in turn, the reduced temporal variability of overall columnar activity. The grand average CSD profiles (Fig. 1) showed a visually distinguishable difference in the temporal flow of cortical processing between ketamine-treated and awake animals. CSD profiles after cortical silencing with topical

application of muscimol demonstrated the early and short synaptic response of thalamic input in layers III/IV and Vb/Vla (Happel *et al.* 2010). The residual sinks after cortical silencing were shorter in duration than before muscimol application. Due to this, much of the following signal represented in the other two conditions could be considered cortical in nature rather than of thalamic origin. This revealed that cortical processing contributes to the peak and duration of early signal processing in the auditory cortex. This could be attributed to recurrent excitation of the stimulus response in cortical layers III/IV (Liu *et al.* 2007). Activity under ketamine, as well as ketamine and topical muscimol, was shown to be fairly stimulus-locked at the area of thalamic input while awake animals have a wider spread of signal response activity across time and space.

To validate that the effects we found across the cortex and in specific layers are significantly above chance (Fig. 2), a cluster-mass permutation test was performed between awake and ketamine-anaesthetized subjects. This revealed significance above chance between groups at a columnar level and most significantly in cortical layer III/IV across early and late time bins. We used analysis of the AVREC in order to determine differences of the overall, temporal columnar response profile (Fig. 3). Single-trial data revealed significantly higher peak amplitude and faster peak latency (Fig. 3B). Due to the difference in the temporal structure of the grand-averaged AVREC traces between both groups (Fig. 3A), we used the



Brown–Forsythe test of variance at the single trial level to observe differences in the stimulus-induced peak responses. The variance of the peak latency of induced activity while awake was significantly higher than under ketamine anaesthesia, whereas the opposite was found for the variance of peak amplitudes (Fig. 4). This increased peak latency variability particularly indicated a different recruitment of cortical cell populations under ketamine, where probabilistic response dynamics were lost.

**Increased recurrent excitation in early granular activity under ketamine**

Ketamine increased recurrent excitation in granular layers after thalamic input to the cortex. Layer-specific tuning curves (Fig. 5) were calculated from a semi-automatic sink detection algorithm in order to further classify the differences found at the columnar level between groups. Significance was revealed in the RMS value around the stimulus response of layer III/IV between

awake and ketamine-anaesthetized gerbils. In contrast, the other layers receiving thalamic input, Vb and VIa, did not show any significant group effects. We inferred based on this result that the input from the thalamus was similar between awake and ketamine-anaesthetized gerbils, which was in accordance with a recent study investigating whole-cell recordings with different sound levels and not finding differential thalamocortical input between conditions (Zhou *et al.* 2014). Therefore, the increased strength seen in granular input layers under ketamine anaesthesia was likely cortically driven – possibly due to ketamine-induced inhibition of GABAergic populations in the granular recurrent feedback loop. Some single and multi-unit studies using ketamine anaesthesia have also specifically implicated a lack of inhibitory modulations from supragranular populations to this recurrent excitation (Wehr & Zador, 2003; Kato *et al.* 2017). This is in line with influences of ketamine on the excitatory and inhibitory balance via selectively reducing activity of PV-releasing GABAergic interneurons. Our

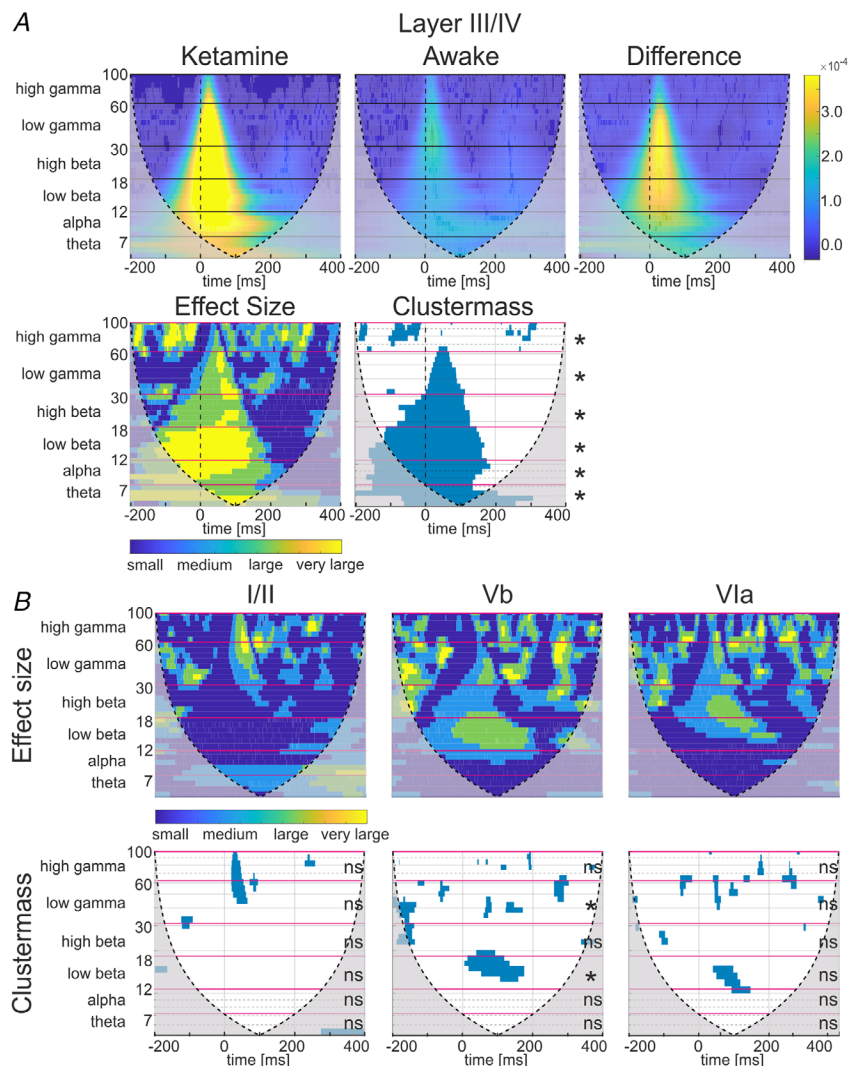


**Figure 6. Magnitude scalograms of continuous wavelet transform and analysis from trial-averaged subject CSD profiles**  
 A, BF response of layer III/IV; scalograms of ketamine group (left,  $n = 11$ ), awake group (middle,  $n = 9$ ), and the absolute difference between both groups (right). Effect size (Cohen's  $d$ ) matrix showing small through very large effect size and clustermass matrix showing significance below  $P < 0.05$  (verified by two-sample Student's  $t$  test). Fuchsia-coloured lines indicate binning borders of frequencies for wavelet analysis and permutation test (left) of the clustermass. B, effect size (Cohen's  $d$ ) matrix, clustermass matrix and permutation test results for layers I/II, Vb and VIa at their respective BF. All graphs show the cone of influence overlaid as a dashed line and muted areas which extend outward. This shows where the wavelet transform was likely affected by boundary conditions. \* $P < 0.05$ , ns: not significant.

data therefore support the hypothesis of ketamine-driven cortical disinhibition (Miller *et al.* 2016) and are in support of previously revealed elevated levels of neural activity after ketamine due to increased cerebral blood flow (Långsjö *et al.* 2005). Furthermore, muscimol silencing strongly reduced the tone-evoked activity in the auditory cortex with a reduced spatiotemporal extent of the granular input sink in accordance with the blocked intracortical local recurrent microcircuits (Fig. 1D; Happel *et al.* 2010). Further studies would be needed to reveal the potential role of NMDA-receptor mediated suppression of GABAergic interneurons or direct effects on excitatory neurons – both suggested before to explain cortical hyper-excitability (Miller *et al.* 2016).

### Boosted recurrent excitation of granular inputs mediates gain enhancement

Ketamine caused stronger granular layer activity leading to a gain increase of cortical input processing (Fig. 5A

and C). This gain increase was significant selectively in granular layers III/IV.

To further explore the phenomenon of layer selective effects, we performed a CWT analysis separately for CSD traces from supragranular layer I/II and thalamic input layers III/IV, Vb and VIa. CWT analysis is ideally suited to analysing the magnitude and phase coherence effects of the peak structure of evoked responses. Performing a clustermass permutation test to compare spectral representations in the awake and ketamine groups, we demonstrated a significant broadband magnitude increase in response to pure-tone stimuli selectively in granular input layers under ketamine (Fig. 6). Ketamine further induced a temporally increased broadband area of cross-trial phase coherence with stronger phase locking of lower frequencies compared to awake recordings (Fig. 7). This finding was consistent with an increase in signal to noise ratio of the phasic response to the auditory stimulus found in granular layers showing a prolonged and enhanced cortical response to pure tones

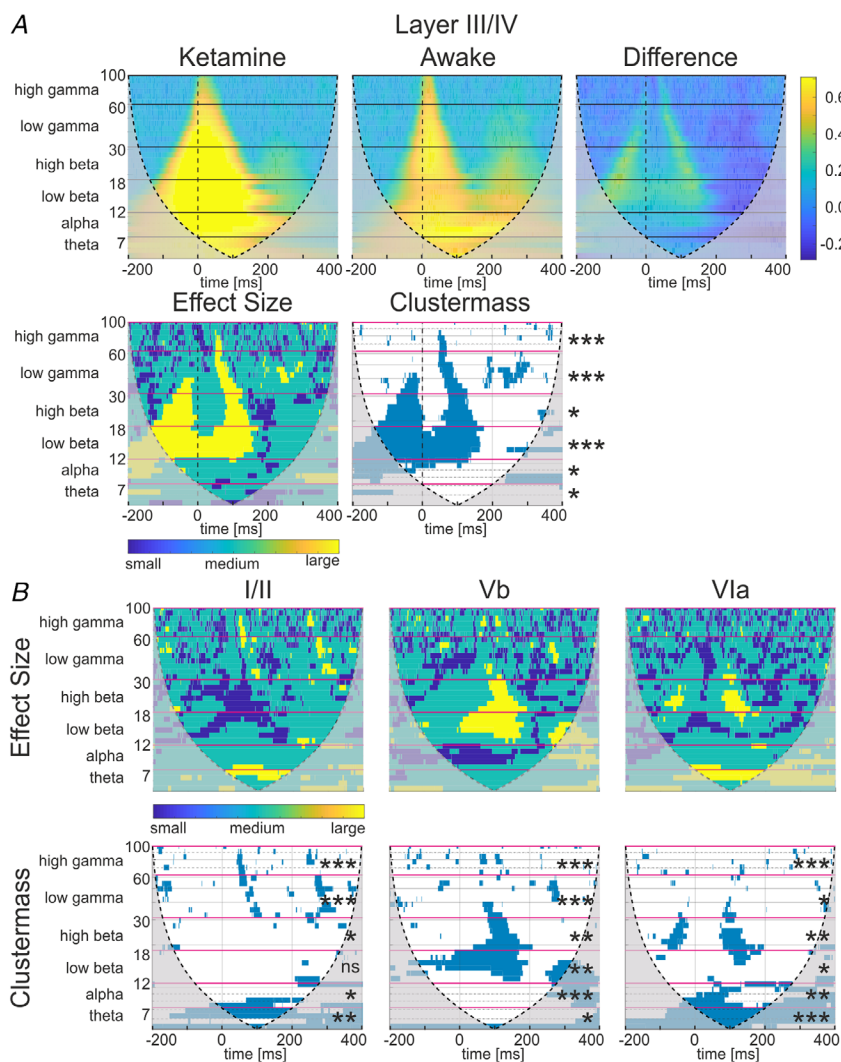


**Figure 7. Phase coherence scalograms of continuous wavelet transform and analysis from single trial subject CSD profiles**

A, BF response of layer III/IV; scalograms of ketamine group (left,  $n = 11$ ), awake group (middle,  $n = 9$ ), and the absolute difference between both groups (right). Effect size matrix showing small through large effect size and clustermass matrix showing significance below  $P < 0.05$  (verified by two-sample Student's  $t$  test). Fuchsia-coloured lines indicate binning borders of frequencies for wavelet analysis and permutation test (left) of the clustermass. B, effect size matrix, clustermass matrix, and permutation test results for layers I/II, Vb and VIa at their respective BF. All graphs show the cone of influence overlaid as a dashed line and muted areas which extend outward. This shows where the wavelet transform was likely affected by boundary conditions. \* $P < 0.05$ , \*\* $P < 0.01$ , \*\*\* $P < 0.001$ , ns: not significant.

(Fig. 1D) as well as the peak amplitude and latency distribution of the AVREC response (Fig. 4A). Enhanced tone-evoked AVREC peak amplitudes together with the less variable peak latencies after ketamine reflected a highly stimulus-locked recruitment of the synaptic circuits in layers III/IV dominating the columnar response to the BF stimulus. For stimulation frequencies at BF  $-2$ , effects were less prominent (data not shown). This indicated that a frequency-specific increase of the recurrent excitation in the granular layer, which is most effectively recruited by salient thalamic input, is the most likely network mechanism by which ketamine affects sensory processing in the cortex.

During early thalamocortical input (*ca* 1–50 ms), granular layer processing showed no significant difference in phase coherence in the frequency range from high beta to high gamma (Fig. 7A), but did demonstrate a broadband increase in phase magnitude (Fig. 6A) between ketamine-anaesthetized and awake groups. Therefore, the granular gain increase under ketamine for these spectral frequencies was mainly due to magnitude effects and not to increased phase coherence. These findings are in accordance with gain enhancement due to an input-circuit-specific dephasing of recurrent excitation and inhibition – otherwise declared as GABAergic disinhibition of recurrent excitation – to incoming external stimuli most prominently seen in the gamma band (Wehr & Zador, 2003; Morita *et al.* 2008; Miller *et al.* 2016).

## Conclusion

Previous findings investigating ketamine *in vivo* have described differential effects based on brain region (Slovik *et al.* 2017; Widman & McMahon, 2018) and method of investigation (Bojak *et al.* 2013; Hildebrandt *et al.* 2017; Schwertner *et al.* 2018), and emphasized the dose dependency of the observed effects (Macdonald *et al.* 1987; Hertle *et al.* 2016; Ahnaou *et al.* 2017). These diverse observations have reported frequency-specific increases or decreases for beta, theta and alpha band oscillations. However, the most robust finding throughout the literature is the increased gamma oscillation across regions and ketamine doses. We have now revealed in our study, that at least for cortical networks, this effect is most robustly explained by a boosted recurrent micro-excitation in granular input layers. The effect was most prominent in granular layers during best-frequency stimulation and less specific for other cortical layers and stimulation frequencies. We therefore propose that effects on lower frequency bands, as also observed across layers and different stimulation frequencies in our study, strongly depend on the very nature of the cortical layer under investigation and type of stimulation. Future studies may therefore enunciate the specificity of higher gamma oscillations for the broadly reported psychological effects

of ketamine, for instance for the development of new therapeutic agents with reduced side effects.

## References

- Ahnaou A, Huysmans H, Biermans R, Manyakov NV & Drinkenburg WHIM (2017). Ketamine: differential neurophysiological dynamics in functional networks in the rat brain. *Transl Psychiatry* **7**, e1237.
- Anis NA, Berry SC, Burton NR & Lodge D (1983). The dissociative anaesthetics, ketamine and phencyclidine, selectively reduce excitation of central mammalian neurones by *N*-methyl-aspartate. *Br J Pharmacol* **79**, 565–575.
- Atencio CA & Schreiner CE (2010). Columnar connectivity and laminar processing in cat primary auditory cortex. *PLoS One* **5**, e9521.
- Barth DS & Di S (1990). Three-dimensional analysis of auditory-evoked potentials in rat neocortex. *J Neurophysiol* **64**, 1527–1536.
- Behrens MM, Ali SS, Dao DN, Lucero J, Shekhtman G, Quick KL & Dugan LL (2007). Ketamine-induced loss of phenotype of fast-spiking interneurons is mediated by NADPH-oxidase. *Science* **318**, 1645–1647.
- Blain-Moraes S, Lee U, Ku S, Noh G & Mashour GA (2014). Electroencephalographic effects of ketamine on power, cross-frequency coupling, and connectivity in the alpha bandwidth. *Front Syst Neurosci* **8**, 114.
- Bojak I, Day HC & Liley DTJ (2013). Ketamine, propofol, and the EEG: A neural field analysis of HCN1-mediated interactions. *Front Comput Neurosci* **7**, 22.
- Brunk MGK, Deane KE, Kisse M, Deliano M, Vieweg S, Ohl FW, Lippert MT & Happel MFK (2019). Optogenetic stimulation of the VTA modulates a frequency-specific gain of thalamocortical inputs in infragranular layers of the auditory cortex. *Sci Rep* **9**, 20385.
- Cardillo G (2009). MWWTEST: Mann-Whitney-Wilcoxon non parametric test for two unpaired samples. <http://www.mathworks.com/matlabcentral/fileexchange/25830>
- Chen CM, Lakatos P, Shah AS, Mehta AD, Givre SJ, Javitt DC & Schroeder CE (2007). Functional anatomy and interaction of fast and slow visual pathways in macaque monkeys. *Cereb Cortex* **17**, 1561–1569.
- Deliano M, Brunk MGK, El-Tabbal M, Zempeltzi MM, Happel MFK & Ohl FW (2020). Dopaminergic neuromodulation of high gamma stimulus phase-locking in gerbil primary auditory cortex mediated by D1/D5-receptors. *Eur J Neurosci* **51**, 1315–1327.
- Deweese MR & Zador AM (2003). Binary coding in auditory cortex. *Adv Neural Inf Process Syst* **15**, 101–108.
- Edeline J-M, Hars B, Hennevin E & Cotillon N (2002). Muscimol diffusion after intracerebral microinjections: A reevaluation based on electrophysiological and autoradiographic quantifications. *Neurobiol Learn Mem* **78**, 100–124.
- Ferguson KA & Cardin JA (2020). Mechanisms underlying gain modulation in the cortex. *Nat Rev Neurosci* **21**, 80–92.
- Fitzgerald PJ & Watson BO (2019). In vivo electrophysiological recordings of the effects of antidepressant drugs. *Exp Brain Res* **237**, 1593–1614.

- Givre SJJ, Schroeder CEE & Arezzo JCC (1994). Contribution of extrastriate area V4 to the surface-recorded flash VEP in the awake macaque. *Vision Res* **34**, 415–428.
- Grent-t-Jong T, Gross J, Goense J, Wibral M, Gajwani R, Gumley AI, Lawrie SM, Schwannauer M, Schultze-Lutter F, Navarro Schröder T, Koethe D, Leweke FM, Singer W & Uhlhaas PJ (2018). Resting-state gamma-band power alterations in schizophrenia reveal E/I-balance abnormalities across illness-stages. *Elife* **7**, E37799.
- Groppe DM, Urbach TP & Kutas M (2011). Mass univariate analysis of event-related brain potentials/fields I: A critical tutorial review. *Psychophysiology* **48**, 1711–1725.
- Grundy D (2015). Principles and standards for reporting animal experiments in *The Journal of Physiology* and *Experimental Physiology*. *J Physiol* **593**, 2547–2549.
- Happel MFK, Jeschke M & Ohl FW (2010). Spectral integration in primary auditory cortex attributable to temporally precise convergence of thalamocortical and intracortical input. *J Neurosci* **30**, 11114–11127.
- Happel MFK & Ohl FW (2017). Compensating level-dependent frequency representation in auditory cortex by synaptic integration of corticocortical input. *PLoS One* **12**, e0169461.
- Heil P (1997a). Auditory cortical onset responses revisited. II. Response strength. *J Neurophysiol* **77**, 2642–2660.
- Heil P (1997b). Auditory cortical onset responses revisited. I. First-spike timing. *J Neurophysiol* **77**, 2616–2641.
- Hertle DN, Heer M, Santos E, Schöll M, Kowoll CM, Dohmen C, Diedler J, Veltkamp R, Graf R, Unterberg AW & Sakowitz OW (2016). Changes in electrocorticographic beta frequency components precede spreading depolarization in patients with acute brain injury. *Clin Neurophysiol* **127**, 2661–2667.
- Hildebrandt KJ, Sahani M & Linden JF (2017). The impact of anesthetic state on spike-sorting success in the cortex: a comparison of ketamine and urethane anesthesia. *Front Neural Circuits* **11**, 95.
- Homayoun H & Moghaddam B (2007). NMDA receptor hypofunction produces opposite effects on prefrontal cortex interneurons and pyramidal neurons. *J Neurosci* **27**, 11496–11500.
- Hubel DH & Wiesel TN (1959). Receptive fields of single neurones in the cat's striate cortex. *J Physiol* **148**, 574–591.
- Hubel DH & Wiesel TN (1962). Receptive fields, binocular interaction and functional architecture in the cat's visual cortex. *J Physiol* **160**, 106–154.
- Hubel DH & Wiesel TN (1965). Receptive field and functional architecture in two nonstriate visual areas (18 and 19) of the cat. *J Neurophysiol* **28**, 229–289.
- Hubel DH & Wiesel TN (1969). Visual area of the lateral suprasylvian gyrus (clare-bishop area) of the cat. *J Neurophysiol* **202**, 251–260.
- Kato HK, Asinof SK & Isaacson JS (2017). Network-level control of frequency tuning in auditory cortex. *Neuron* **95**, 412–423.e4.
- Kaur S, Lazar R & Metherate R (2004). Intracortical pathways determine breadth of subthreshold frequency receptive fields in primary auditory cortex. *J Neurophysiol* **91**, 2551–2567.
- Lachaux J-P, Rodriguez E, Martinerie J & Varela FJ (1999). Measuring phase synchrony in brain signals. *Hum Brain Mapp* **8**, 194–208.
- Långsjö JW, Maksimow A, Salmi E, Kaisti K, Aalto S, Oikonen V, Hinkka S, Aantaa R, Sipilä H, Viljanen T, Parkkola R & Scheinin H (2005). S-Ketamine anesthesia increases cerebral blood flow in excess of the metabolic needs in humans. *Anesthesiology* **103**, 258–268.
- Lazarewicz MT, Ehrlichman RS, Maxwell CR, Gandal MJ, Finkel LH & Siegel SJ (2010). Ketamine modulates theta and gamma oscillations. *J Cogn Neurosci* **22**, 1452–1464.
- Lilly JM & Olhede SC (2012). Generalized morse wavelets as a superfamily of analytic wavelets. *IEEE Trans Signal Process* **60**, 6036–6041.
- Liu B, Wu GK, Arbuckle R, Tao HW & Zhang LI (2007). Defining cortical frequency tuning with recurrent excitatory circuitry. *Nat Neurosci* **10**, 1594–1600.
- Luczak A & Maclean JN (2012). Default activity patterns at the neocortical microcircuit level. *Front Integr Neurosci* **6**, 30.
- Ma L, Skoblenick K, Johnston K & Everling S (2018). Ketamine alters lateral prefrontal oscillations in a rule-based working memory task. *J Neurosci* **38**, 2482–2494.
- Macdonald JF, Miljkovic Z & Pennefather P (1987). Use-dependent block of excitatory amino acid currents in cultured neurons by ketamine. *J Neurophysiol* **58**, 251–266.
- Maris E, Schoffelen JM & Fries P (2007). Nonparametric statistical testing of coherence differences. *J Neurosci Methods* **163**, 161–175.
- Metherate R, Kaur S, Kawai H, Lazar R, Liang K & Rose HJ (2005). Spectral integration in auditory cortex: Mechanisms and modulation. *Hear Res* **206**, 146–158.
- Michelson NJ & Kozai TDY (2018). Isoflurane and ketamine differentially influence spontaneous and evoked laminar electrophysiology in mouse V1. *J Neurophysiol* **120**, 2232–2245.
- Miller OH, Moran JT & Hall BJ (2016). Two cellular hypotheses explaining the initiation of ketamine's antidepressant actions: Direct inhibition and disinhibition. *Neuropharmacology* **100**, 17–26.
- Mitzdorf U (1985). Current source-density method and application in cat cerebral cortex: Investigation of evoked potentials and EEG phenomena. *Physiol Rev* **65**, 37–100.
- Morita K, Kalra R, Aihara K & Robinson HPC (2008). Recurrent synaptic input and the timing of gamma-frequency-modulated firing of pyramidal cells during neocortical "UP" states. *J Neurosci* **28**, 1871–1881.
- Olhede SC & Walden AT (2002). Generalized Morse wavelets. *IEEE Trans Signal Process* **50**, 2661–2670.
- Pachitariu M, Lyamzin DR, Sahani M & Lesica NA (2015). State-dependent population coding in primary auditory cortex. *J Neurosci* **35**, 2058–2073.
- Pallavicini C, Vilas MG, Villarreal M, Zamberlan F, Muthukumaraswamy S, Nutt D, Carhart-Harris R & Tagliazucchi E (2019). Spectral signatures of serotonergic psychedelics and glutamatergic dissociatives. *Neuroimage* **200**, 281–291.
- Petersen CCH, Grinvald A & Sakmann B (2003). Spatiotemporal dynamics of sensory responses in layer 2/3 of rat barrel cortex measured in vivo by voltage-sensitive dye imaging combined with whole-cell voltage recordings and neuron reconstructions. *J Neurosci* **23**, 1298–1309.

- Qi R, Li J, Wu X, Geng X, Chen N & Yu H (2018). Effects of ketamine on basal gamma band oscillation and sensory gating in prefrontal cortex of awake rats. *Neurosci Bull* **34**, 457–464.
- Sakata S & Harris KD (2009). Laminar structure of spontaneous and sensory-evoked population activity in auditory cortex. *Neuron* **64**, 404–418.
- Schaefer MK, Hechavarría JC & Kössl M (2015). Quantification of mid and late evoked sinks in laminar current source density profiles of columns in the primary auditory cortex. *Front Neural Circuits* **9**, 52.
- Schobel SA, Chaudhury NH, Khan UA, Paniagua B, Styner MA, Asllani I, Inbar BP, Corcoran CM, Lieberman JA, Moore H & Small SA (2013). Imaging patients with psychosis and a mouse model establishes a spreading pattern of hippocampal dysfunction and implicates glutamate as a driver. *Neuron* **78**, 81–93.
- Schroeder C, Mehta AD & Givre SJ (1998). A spatiotemporal profile of visual system activation revealed by current source density analysis in the awake macaque. *Cereb Cortex* **8**, 575–592.
- Schwertner A, Zortea M, Torres FV & Caumo W (2018). Effects of subanesthetic ketamine administration on visual and auditory event-related potentials (ERP) in humans: A systematic review. *Front Behav Neurosci* **12**, 70.
- Slovik M, Rosin B, Moshel S, Mitelman R, Schechtman E, Eitan R, Raz A & Bergman H (2017). Ketamine induced converged synchronous gamma oscillations in the cortico-basal ganglia network of nonhuman primates. *J Neurophysiol* **118**, 917–931.
- Steinschneider M, Reser DH, Fishman YI, Schroeder CE & Arezzo JC (1998). Click train encoding in primary auditory cortex of the awake monkey: Evidence for two mechanisms subserving pitch perception. *J Acoust Soc Am* **104**, 2935–2955.
- Steinschneider M, Tenke CE, Schroeder CE, Javitt DC, Simpson GV, Arezzo JC & Vaughan HG (1992). Cellular generators of the cortical auditory evoked potential initial component. *Electroencephalogr Clin Neurophysiol Potentials Sect* **84**, 196–200.
- Supp GG, Siegel M, Hipp JF & Engel AK (2011). Cortical hypersynchrony predicts breakdown of sensory processing during loss of consciousness. *Curr Biol* **21**, 1988–1993.
- Szymanski FD, Garcia-Lazaro JA & Schnupp JWH (2009). Current source density profiles of stimulus-specific adaptation in rat auditory cortex. *J Neurophysiol* **102**, 1483–1490.
- Wehr M & Zador AM (2003). Balanced inhibition underlies tuning and sharpens spike timing in auditory cortex. *Nature* **426**, 442–446.
- Widman AJ & McMahon LL (2018). Disinhibition of CA1 pyramidal cells by low-dose ketamine and other antagonists with rapid antidepressant efficacy. *Proc Natl Acad Sci U S A* **115**, E3007–E3016.
- Zhang Y, Wu S, Xie L, Yu S, Zhang L, Liu C, Zhou W & Yu T (2019). Ketamine within clinically effective range inhibits glutamate transmission from astrocytes to neurons and disrupts synchronization of astrocytic SICs. *Front Cell Neurosci* **13**, 240.
- Zhou M, Liang F, Xiong XR, Li L, Li H, Xiao Z, Tao HW & Zhang LI (2014). Laminar-specific scaling down of balanced excitation and inhibition by active behavioral states in auditory cortex. *Nat Neurosci* **17**, 841–850.

## Additional information

### Competing interests

There were no conflicts of interest in this study.

### Author contributions

Research was performed in the laboratories of the Leibniz-Institute for Neurobiology, Magdeburg (Germany), and designed by K.E.D. and M.F.K.H. M.F.K.H. supervised the project. Experiments were performed by K.E.D., M.G.K.B., J.M., X.L., M.M.Z., F.A. and S.A. and supervised by M.F.K.H. and M.D. Data were analysed by K.E.D., M.G.K.B., A.W.C. and M.M.Z. Statistical analysis was performed by K.E.D. Figures were prepared by K.E.D. and A.W.C. K.E.D. wrote the initial paper draft. Manuscript was written by K.E.D. and M.F.K.H. with the assistance from M.G.K.B., M.D. and F.W.O. All authors have read and approved the final version of this manuscript and agree to be accountable for all aspects of the work in ensuring that questions related to the accuracy or integrity of any part of the work are appropriately investigated and resolved. All persons designated as authors qualify for authorship, and all those who qualify for authorship are listed.

### Funding

This project was funded by the Deutsche Forschungsgemeinschaft (DFG SFB 779; M.F.K.H., F.W.O.), the Leibniz Association (W.G.L.; Leibniz Postdoctoral Network, M.F.K.H.), and the China Scholarship Council (CSC No. 201506290028; X.L.; CSC No. 201408430074; J.M.).

### Acknowledgements

We would like to thank Kathrin Ohl and Silvia Vieweg for their technical assistance.

### Keywords

auditory cortex, continuous wavelet analysis, current source density, ketamine anaesthesia, laminar recording, mesoscopic, microcircuitry, population dynamics

### Supporting information

Additional supporting information may be found online in the Supporting Information section at the end of the article.

### Statistical Summary Document

### Github repository for scripts and data used